Visualizing a one-way protein encounter complex by ultrafast single-molecule mixing

Yann Gambin[1,2,5], **Virginia Vandelinder**[3,4,6], **Allan Chris M. Ferreon**[1,6], **Edward A. Lemke**[1,4], **Alex Groisman**[3,5], and **Ashok A. Deniz**[1,5]

[1] Dept of Molecular Biology, The Scripps Research Institute, La Jolla, CA, USA

[3] Dept of Physics, University of California San Diego, San Diego, CA, USA

Abstract

We combined rapid microfluidic mixing with single-molecule Förster Resonance Energy Transfer to study the folding kinetics of the intrinsically disordered human protein α-synuclein. The time-resolution of 0.2 ms revealed initial collapse of the unfolded protein induced by binding with lipid-mimics and subsequent rapid formation of transient structures within the encounter complex. The method also enabled study of rapid dissociation and unfolding of weakly bound complexes triggered by massive dilution.

α-Synuclein is an intrinsically-disordered protein (IDP) whose folding is not solely encoded by its amino acid sequence but rather depends on its binding to other proteins or membranes in the cell. A general open question for such IDPs is whether binding is initiated by formation of transient structures in the unfolded protein, or whether folding is only induced after contact with binding partners 1. These two scenarios can be distinguished more directly using single-molecule methods, which avoid averaging the measurements of properties over many proteins. In particular, single-molecule Förster Resonance Energy Transfer (smFRET) is a tool of choice for direct observation of folding pathways 2. When used in combination with a kinetic mixing apparatus to rapidly trigger transitions, smFRET can reveal the sequence of binding and folding steps, and uncover intermediate conformations that are only transiently formed.

Advances in microfluidic mixing technology during the last decade3,4 have resulted in devices with enhanced capabilities for studies of early events in protein folding 5,6,7. However, accessing early steps during non-equilibrium folding with smFRET is a technical

[5]Correspondence should be addressed to: y.gambin@imb.uq.edu, agroisman@ucsd.edu, deniz@scripps.edu.
[2]Current Address: Institute for Molecular Bioscience, University of Queensland, Brisbane, Australia
[4]Current Address: Structural and Computational Biology Unit, European Molecular Biology Laboratory, Heidelberg, Germany.
[6]These authors contributed equally

Supplementary Note. Operation and characterization of the device

challenge. The key problem is that existing microfluidic setups rely on high flow velocities to rapidly trigger conformational changes. For example, in order to reach the fastest mixing times (<10 μs), laminar sheath-flow microfluidic mixers typically require 1–10 m/s flow velocities[3,4], which are incompatible with smFRET, because a fluorescently labeled protein needs to spend enough time in the focal volume for sufficient photons to be collected. In recent years, several microfluidic setups have been specially designed for smFRET measurements at low flow velocities with improved time resolution[8–10]. Nevertheless, the earliest protein folding events reported so far have been at relatively long times on the order of ~10 ms[11,12], far from the current limit for smFRET time-resolution of ~100 μs.

To detect folding events on the 200 μs–100 ms timescale, we built a microfluidic device that creates an abrupt flow deceleration, allowing high-speed laminar mixing to be followed by smFRET detection in a slow flow (Fig. 1a–g and Supplementary Figs. 1–13). In the mixing region of the device (Fig. 1b,c), two high-speed buffer streams squeeze the protein stream into a layer as narrow as ~20 nm (Supplementary Note). Ligands and other small molecules diffuse rapidly across this layer and trigger protein transitions. Immediately downstream of the mixing region, >99.5% of the flow is abruptly diverted into two side outlets at a four-way junction (Fig. 1c). The four-way junction was optimized by extensive 3D flow simulations to prevent vortices and flow instabilities. The protein flow abruptly decelerates and expands, and some of its streamlines the junction and make >90° turns curling back towards the side channels. The inertia of the protein stream makes it diverge in the *z*-direction (Fig. 1g). Hence, nearly all protein molecules interrogated with smFRET travel along the channel centerline and have uniform passage times through the mixing region. This diversion causes the sample flow velocity to decrease by ~3 orders of magnitude from a peak value of ~2m/s within ~10 μm distance, resulting in an only ~200 μs dead-time (Fig. 1d) between the medium exchange and earliest smFRET measurements(Fig. 1d).

We employed this device with improved mixing time-resolution to investigate the coupled binding and folding of α-synuclein using smFRET. Previous studies showed that interaction with negatively charged lipid bilayers can transform α-synuclein from a disordered (**U**) to a folded extended helix (**F**) state, and that the lipid-mimic SDS can reproduce this behavior [13]. Here, we used SDS monomers as binding partners to explore the kinetic folding and unfolding paths between **U** and **F** states.

To test its conformations with smFRET, we labeled α-synuclein with donor (Alexa488) and acceptor (Alexa594) dyes at positions 7 and 84 [14]. The microfluidic device was mounted on a home-built confocal setup with two detectors that simultaneously recorded bursts of fluorescence as individual labeled proteins passed through the confocal volume. Donor and acceptor photon counts were analyzed to generate histograms of FRET efficiency, E_{FRET}, which translated into structural distributions [2,14]. By placing the confocal volume at different points along the detection region (Fig. 1c,d), we followed the evolution of α-synuclein E_{FRET} distributions from 200 μs to >100 ms after mixing (Fig. 2a–c).

We first used the microfluidic device to rapidly change the buffer of unfolded α-synuclein (**U**) to a solution promoting formation of the **F** state. This solution contained 1.2 mM of the binding partner SDS and 20 μM of unlabeled α-synuclein, as in a previous study [14].

Strikingly, multiple folding events were observed en route from **U** to **F** (Fig. 2a, Supplementary Figs. 14–21). The earliest smFRET measurement, at only 200 μs after the addition of SDS, already showed a shift of the histogram peak from 0.42 (**U** state in the absence of SDS) towards higher E_{FRET}. Hence, rather than causing an expansion of the protein chain as expected for a direct **U** to **F** transition, interaction of the protein with negatively charged SDS molecules initially leads to a rapid collapse (Supplementary Figs. 14 and 15). Following this initial compaction (E_{FRET} ~0.6 at 500 μs), we observed a break in the shift of the FRET peak and a transition towards a high E_{FRET} intermediate state (**I** with E_{FRET} ~0.8), fully formed after 1 ms. In the next 11 ms, this intermediate is converted in a two-state process to the expected final **F** state structure characterized by a low-E_{FRET} peak (see Fig. 2c for individual histograms, and Supplementary Figs. 16–21 for further analysis of transitions).

Observation of these multiple steps during folding to **F** raises an interesting question: are similar intermediate states observed during the conversion of **F** back to **U** when protein-SDS complexes dissociate? To address this question, we used another powerful feature of the microfluidic device: the ability to continuously and rapidly vary the concentration of labeled protein in the detection region. The technique takes advantage of the lateral diffusion (dilution) of proteins out of their squeezed, narrow stream while they travel through the mixing region. By applying slightly asymmetric flow rates of the two buffer streams, we can steer the middle of the focused stream away from the detection region and direct there a solution with greatly reduced protein concentration, thus diluting a protein sample by a factor as high as 10^6 within ~200 μs (Supplementary Fig. 11 and Supplementary Note).

For this unfolding experiment (Fig. 2b), we used a concentration of labeled proteins in the SDS-protein buffer that favor the **F** state. The SDS-protein solution was hydrodynamically focused between streams of buffer lacking SDS or protein. We tuned the asymmetry of the buffer streams to dilute the SDS-synuclein complexes by >100-fold, thus triggering rapid dissociation of binding partners and protein unfolding. The low-E_{FRET} **F**-peak present at 200 μs disappeared after ~1 ms with concomitant formation of a **U**-peak indicating that the weakly-bound complexes dissociated rapidly and a simple 2-state transition occurred. Interestingly, no folding intermediates with high E_{FRET} were observed on the unfolding pathway (Fig. 2b,c and Supplementary Figs. 22, 23).

The smFRET kinetic data suggest the following α-synuclein binding-folding scenario (Fig. 2d). At early stages, binding of SDS molecules to the unfolded α-synuclein collapses the protein; the continuous shift of the E_{FRET} peak suggests that we observe an "encounter complex" that precedes formation of large-scale structures. The folding of α-synuclein is induced within the complex, and proceeds by way of a partly folded intermediate state. The FRET peak of this intermediate closely resembles the FRET peak observed previously for the protein bound to SDS micelles in a helix-kink-helix structure [13,14]. This "broken helix" conformation was previously believed to be an artifact of highly curved micelles, with an elongated helix being the relevant membrane-stabilized state. The data in Fig. 2a,c now show that the broken helix structure may be relevant as an essential kinetic step in the process of folding towards the membrane-bound extended helix.

Another interesting observation is that the folding from **U** to **F** and unfolding from **F** to **U** follow radically different pathways (Fig. 2d). On a molecular level, it opens an intriguing possibility: the intermediate folding step suggests that not all "binding sites" are readily accessible within the unfolded α-synuclein. Even if the protein does not have a stable structure under native conditions, its spatial conformation may not be fully random and some sites of the protein chain could be concealed to binding partners due to intra-chain interactions. These sites would only be exposed after the formation of the intermediate folded state, allowing partners to bind to the protein, thus inducing the final conformational switch. In contrast, when the binding partners are rapidly removed from the fully-folded state, the different SDS sites may exhibit similar high dissociation rates, resulting in rapid and random loss of overall structure and a fast collapse with no detectable intermediates.

The single-molecule microfluidic mixer described here enabled detailed mapping of the binding-induced folding kinetics of α-synuclein. It revealed transient conformations and steps that would have remained hidden in both bulk and single-molecule experiments using existing instrumentation. The device brings the time resolution of smFRET kinetics close to the physical limit imposed by current fluorescent dyes, as the latency of 200 μs is nearly the same as the minimal time required to collect sufficient photons[15]. Moreover, the rapid and massive dilution capability of the device provides the ability to study weakly bound complexes and transient oligomers, which usually dissociate quickly at single-molecule concentrations.

Methods

Microfluidic Device Design

The microfluidic device is designed to provide fast and efficient medium exchange in a laminar sheath flow in its mixing region and abrupt deceleration of the sample stream at a four-way junction, which is situated immediately upstream of its detection region. The shape of channels in the device and flow conditions in the detection region are optimized for single-molecule FRET (smFRET) spectroscopy, as shown in Supplementary Fig. 1.

Similarly to the previous microfluidic hydrodynamic focusing mixers, the buffer exchange in the mixing region occurs by molecular diffusion between a thin sample stream, which is sandwiched between two buffer streams in a laminar sheath flow. However, unlike previous designs, the mixing region is separated from the detection region, where smFRET interrogation is performed, and the flow speeds in these two regions can be adjusted independently by varying the part of flow diverted into two side channels at the four-way junction between the mixing and detection regions. Typically, ~99.8% of flow in the mixing region is diverted to the side channels, leading to ~3 orders of magnitude reduction of flow velocity in the detection region as compared with the mixing region. This mode of operation makes it possible to combine rapid buffer exchange in a fast flow in the mixing region (velocities up to 2m/s) with smFRET detection in a slow flow in the detection region (velocities of a few mm/s). Importantly, the deceleration of the sample flow from the high velocities in the mixing region to the low velocities in the detection region occurs over a short distance, leading to a short deceleration time (in the Lagrangian reference frame of the moving liquid) and small dead time between mixing and smFRET detection. Small dead

times provided by the device made it possible to access sub-millisecond timescales (comparable to those in stopped-flow instruments) in a system that requires a very small amount of sample and is compatible with high numerical aperture (high NA) confocal optical setup and high photon efficiency smFRET detection.

The device also makes it possible to take advantage of the lateral diffusion of the sample molecules in the mixing region, with characteristic lateral diffusion distances of ~0.1 μm during ~100 μs long passage through the mixing region. It is worth noting that with the typical initial sample stream width of ~20 nm, this diffusive broadening causes a major change in the distribution of concentration across the stream, bringing a large part of the sample molecules outside of geometrical boundaries of the stream. (Those boundaries can be defined as boundaries in the absence of diffusion.) The nearly 3 orders of magnitude deceleration of the sample stream at the transition from the mixing to the detection region leads to >2 orders of magnitude magnification of distances across the stream in the lateral direction. (There is also some expansion of the stream and concomitant increase of distances in the out-of-plane direction, as shown in Fig. 1 in the main text and in Supplementary Fig. 12) As a result, in the detection region, the characteristic length scale of sample concentration variations across the stream becomes >10 μm, making the sample concentration nearly uniform within the focal volume of the smFRET setup (~0.3 μm in diameter). This feature makes it possible to selectively interrogate parts of the sample stream with molecules that diffused particularly far from the geometrical boundaries of the sample stream in the mixing region and with sample concentration dramatically reduced compared with the original sample solution. A part of the sample stream with a desired sample concentration is directed into the detection region by adjusting the flow rates of the two focusing buffer streams to steer the center of the sample stream somewhat away from the detection region. With this technique, a protein sample can be diluted by factors as high as 10^6 within <1 ms. Importantly, the flow towards the two side channels at the four-way junction is kept symmetric to prevent flow instabilities.

Device measurement timescales

The device has three smFRET measurement areas. Before entering the mixing region, the sample solution passes through a wide chamber where the flow is sufficiently slow for smFRET to be essentially diffusion-limited. After exiting the mixing region, the sample flows through a 5 mm long detection region (Supplementary Fig. 1c). At normal device operation conditions, the most upstream and the most downstream smFRET measurement points in this region correspond, respectively, to ~200 μs and ~1 s from the time of buffer exchange, making the entire range from 200 μs to ~1 s accessible in a single experiment. Special markers in the microfluidic chip positioned every 100 μm along the detection region help to determine the precise distance of a given measurement point from the detection region entrance (blue box, Supplementary Fig. 1c). The detection region is connected to the protein outlet by a long serpentine channel, which makes it possible to access protein conformations over an extended time range (up to 5 min, at reduced flow rates) by measuring smFRET at various points along the serpentine channel (red box, Supplementary Fig. 1c). After ~100 ms, substantial uncertainty is introduced into the distance-time conversion due to the combined effect of diffusion of sample molecules across the channels

and parabolic profile of velocity of the laminar flow in the detection region and in the serpentine channel. Nevertheless, measurements at large reaction times still provide information on "equilibrium" protein conformations and semi-quantitative data on the kinetics of slow folding processes.

Device channel dimensions

The choice of the channels depth was dictated by multiple considerations. Channels with small diameters are preferable for reducing the time of deceleration and the measurement dead time, giving access to better time resolution. In addition, small channel dimensions lead to small values of the Reynolds number, Re, at a given flow speed, making the flow more stable and less prone to vortex buildup near corners. On the other hand, channels with small diameters result in high flow resistances, making it difficult to combine high flow velocity in the mixing region (e.g. 2m/s) with low driving pressure (preferably 4 psi to prevent large deformations of soft PDMS walls and separation of the PDMS chip from the substrate). Small channels are also more difficult and costly to fabricate and more prone to clogging, especially when their diameters are less than a few microns. Lastly, performing measurements with the confocal volume close to walls may be detrimental to smFRET signal quality. In particular, in early device designs, we noticed high levels of autofluorescence near channel bottoms, apparently due to the proximity to the borosilicate cover glass substrate. This autofluorescence significantly contributed to the smFRET background for distances up to 20 microns from the glass surface.

We found a uniform channel depth of 15 microns to be a reasonable choice, making it possible to reach sufficiently short reaction dead times and suppress vortexes without using excessively high driving pressure.

The problem of cover glass autofluorescence was resolved by bonding the microfluidic chips to cover glasses coated with a 50 μm layer of PDMS. The autofluorescence of PDMS at the wavelength used in the experiments was much lower than that of glass (2 counts/ms vs. 20 count/ms). Therefore, the PDMS layer on the cover glass considerably reduced the noise and allowed clean smFRET measurements in channels as shallow as 10 microns without using expensive fused silica cover glasses as substrates.

If not adjusted for, the addition of a PDMS layer on a cover glass can lead to spherical aberrations in the optical setup, reducing the confocality and the efficiency of light focusing and collection. When, as in the present study, a water immersion (WI) objective is used, the spherical aberrations originate from the difference between the refractive index of PDMS ($n_p = 1.41$) and water ($n_w = 1.33$), $n_p = n_p - n_w = 0.08$. These aberrations are of the same nature as the spherical aberrations resulting from the difference between the refractive index of glass ($n_p = 1.51$) and water, $n_g = n_p - n_w = 0.18$, and a mismatch between the actual thickness of the cover glass and the cover glass thickness the objective is optimized for. In terms of spherical aberrations, the addition of a PDMS layer with a thickness $d = 50$ μm is nearly equivalent to the addition of $d' = d \cdot n_p / n_g = 22$ μm of cover glass thickness. Therefore, to correct for the PDMS layer, we set the correction collar to a cover glass thickness 0.02 mm greater that the actual thickness of the cover glass. Specifically, for #1

cover glasses used in the experiments, the correction collar was set to a thickness of 0.17 mm, corresponding to a #1.5 cover glass.

In order to check that the smFRET data were not affected by the possible changes in focusing and light collection, we compared histograms of FRET efficiencies for two different folded states, in the device with PDMS-coated cover glass and in a cuvette with a plain glass bottom (Supplementary Fig. 13). No data degradation was found in the device vs. cuvette, which was consistent with the absence of appreciable optical aberrations in the experiment in the device.

The width of the channel in the detection region was chosen at 25 μm, so the beams focused and collected by the high-NA objective used in the experiments (63X/1.2NA water immersion) would not be distorted by passing through the PDMS side-walls of the channel, which had a refractive index of ~1.41 as compared to 1.33 for water. The lengths and widths of other channels were selected to obtain a desired range of flow velocities in the mixing and detection regions within a convenient range of driving pressures applied to the device inlets.

Device Fabrication

The microfluidic chip is a poly(dimethylsiloxane) (PDMS; Sylgard 184 (Dow Corning)) cast of a UV-lithography microfabricated master mold. To make the master mold, a 15 μm layer of UV-curable epoxy SU8 2015 (MicroChem) was spin-coated onto a 5″ silicon wafer, exposed to UV-light through a specially designed chrome photomask (Photo Sciences, Inc.; 0.5 μm resolution), cured on a hot plate, and developed. The resulting master mold was silanized by exposure to a vapor of chlorotrimethylsilane (Sigma-Aldrich) at room temperature for 90 s to facilitate release of the PDMS replicas. Next, PDMS pre-polymer was poured onto the master mold and baked at 80°C for 1 hr. The PDMS casts (~5 mm thick) were peeled off the master mold and cut into individual chips, which were trimmed to size and punched with luer stubs to make inlet and outlet holes. PDMS-coated cover glasses were made by spin-coating a 50 μm thick layer of PDMS pre-polymer on #1 microscope cover glasses and baking the cover glasses at 80°C for 1 hr. The microfabricated PDMS chips were then reversibly bonded to the PDMS-coated cover glasses by overnight baking in an 80°C oven. The PDMS-PDMS bond withstood pressures as high as 7 psi in the device without delamination (higher pressures were not tested since 7 psi was more than sufficient for our experiments). The master mold had 4 copies of the device, and a single master mold was used for making all the PDMS casts. Devices were cleaned by boiling in 0.1 M HCl for 1 hr and then bonded to fresh PDMS-coated cover glasses for repeated use. We are willing to assist with technical advice to facilitate utilization of the device and technique by other research groups, and to provide devices for testing in specific cases as feasible.

Protein Expression, Purification and Labeling

Mutagenesis, expression and purification of mutant proteins were carried out following the procedure described previously (13). The plasmid construct for wildtype α-synuclein was kindly provided by R. L. Nussbaum (National Institutes of Health, Bethesda, MD). Preparation of labeled protein was carried out as reported previously (14). Briefly, the G7,84C cysteine mutant was sequentially reacted with Alexa Fluor 488 maleimide (donor)

and Alexa Fluor 594 maleimide (acceptor) dyes (Molecular Probes, Inc.). Monomerically labeled protein was purified after the first step of donor labeling, and this was followed by labeling with an excess of acceptor dye, and another round of purification. Protein identity and purity were ascertained by HPLC and Mass Spectrometry analyses.

Single-molecule FRET measurements

Single-molecule FRET measurements were performed as previously described (14). Briefly, experiments were carried out on a laser confocal microscope system home-built around an Axiovert 200 microscope (Zeiss). Excitation of single molecules was achieved by focusing a beam derived from the 488 nm line of a 543-AP-A01 tunable argon-ion laser (Melles Griot) inside the sample solution, 7.5μm from the surface of the PDMS layer on a #1 cover glass, using a water immersion objective (1.2 NA, 63X, Zeiss). Donor and acceptor single-molecule fluorescence signals were collected through the same objective, were separated from the excitation light by using a dichroic mirror (Q495LP, Chroma Tech. Corp.), and spatially filtered using a 100 μm pinhole. A second dichroic mirror (560 DCXR, Chroma)was then used to separate donor and acceptor emission components, which were further filtered using an HQ 525/50M band-pass filter (donor, Chroma) and a 590 LPV2 long-pass filter (acceptor, Chroma), respectively. These photon streams were then detected using two SPCM-AQR-14 avalanche photodiode (APD) photon counting modules (Perkin-Elmer Optoelectronics). Photon counts were recorded with a counter card (PCI 6602, National Instruments) interfaced with a computer using a code in LabView (National Instruments).

The FRET efficiency histograms reported in the paper were generated by using a two-channel data collection mode to record donor and acceptor light intensities (photon counts) as functions of time. To ensure that virtually all of the detected photon bursts were from single α-synuclein molecules, the concentration of donor-acceptor solutions in the detection region was~100 pM (in fluorophore concentration). The protein sample solution also contained a higher concentration of unlabeled α-synuclein to avoid the strong effect of even very low concentrations of SDS micelles on labeled synuclein conformation by rebalancing the stoichiometries of the SDS and synuclein, as discussed previously (13, 14). We note that control experiments in a previous paper (6) using the concentration dependence of synuclein-SDS binding-folding excluded measurable association/aggregation. Hence, the observations reflect intrinsic monomer folding/unfolding properties. In addition, the molecules interrogated by smFRET travel near the centerline of the channel, minimizing the effect of their interaction with channel walls. The background counts, leakage of donor into acceptor channel (~8%) and the direct excitation of acceptor (~5%) were used to correct the signals before calculating FRET efficiencies.

A threshold of 40 counts (the sum of the photon counts from the two channels) was used to separate the photon burst events due to fluorescently labeled protein molecules from background. Ratiometrically-measured FRET efficiencies (E_{FRET}) are defined on the basis of the measured donor (I_D) and acceptor (I_A) fluorescence intensities as:

$$E_{FRET} = \frac{I_A}{I_A + \gamma I_D}$$

γ is a correction factor dependent on the donor (Φ_D) and acceptor (Φ_A) quantum yields, and the donor channel (η_D) and acceptor channel (η_A) detection efficiencies, defined as:

$$\gamma = \frac{\eta_A \Phi_A}{\eta_D \Phi_D}$$

For the dual-labeled α-synuclein molecules used in the study, γ was previously found to be close to 1; this value used here. FRET efficiencies were calculated for each validated event and plotted in the form of a histogram.

At least 10 measurements were made for each position, *x*, along the detection region of the microfluidic device to construct a FRET histogram representing at least 2,000 different molecules; the smFRET three-dimensional map displayed in Fig. 2 in the main text was compiled from twenty three separate histograms taken at different reaction time points (different positions along the detection region), representing a total of more than 50,000 individual events. The histograms were fitted with Gaussian functions using Origin (OriginLab Corp., Northampton, MA), IGOR (WaveMetrics, Lake Oswego, OR) and Microsoft Excel, and the peak positions and areas under the peaks were obtained from the fitting parameters.

We verified in previous work that the **F**-state results in a low E_{FRET} peak, which can be distinguished from the zero-peak using alternating excitation of the donor and acceptor dyes (14). Here, for the cases with F-state, the zero-peak parameters were fixed, allowing the **F**-state to be fitted.

Additional details of the device operation and full characterization, as well as smFRET measurements and analysis are presented in the Supplementary Note and Supplementary Figs. 1–23.

Supplementary Material

Refer to Web version on PubMed Central for supplementary material.

Acknowledgments

References

1. Wright PE, Dyson HJ. Curr Opin Struct Biol. 2009; 19:31. [PubMed: 19157855]

2. Deniz AA, Mukhopadhyay S, Lemke EA. J R Soc Interface. 2008; 5:15. [PubMed: 17519204]

3. Knight JB, et al. Phys Rev Lett. 1998; 80:3863.

4. Hertzog DE, et al. Anal Chem. 2006; 78:4299. [PubMed: 16808436]

5. Pollack L, et al. Proc Natl Acad Sci USA. 1999; 96:10115. [PubMed: 10468571]

6. Hoffmann A, et al. Proc Natl Acad Sci USA. 2007; 104:105. [PubMed: 17185422]

7. DeCamp SJ, et al. Biophys J. 2009; 97:1772. [PubMed: 19751683]

8. Lipman EA, et al. Science. 2003; 5637:1233. [PubMed: 12947198]

9. Lemke EA, et al. J Am Chem Soc. 2009; 131:13610. [PubMed: 19772358]

10. Pfeil SH, et al. Rev Sci Instrum. 2009; 80:055105. [PubMed: 19485532]

11. Hamadani KM, Weiss S. Biophys J. 2008; 95:352. [PubMed: 18339751]

12. Hofmann H, et al. Proc Natl Acad Sci USA. 2010; 107:11793. [PubMed: 20547872]

13. Ferreon ACM, Deniz AA. Biochemistry. 2007; 46:4499. [PubMed: 17378587]

14. Ferreon ACM, et al. Proc Natl Acad Sci USA. 2009; 106:5645. [PubMed: 19293380]

15. Chung HS, Louis JM, Eaton WA. Proc Natl Acad Sci USA. 2009; 106:11837. [PubMed: 19584244]
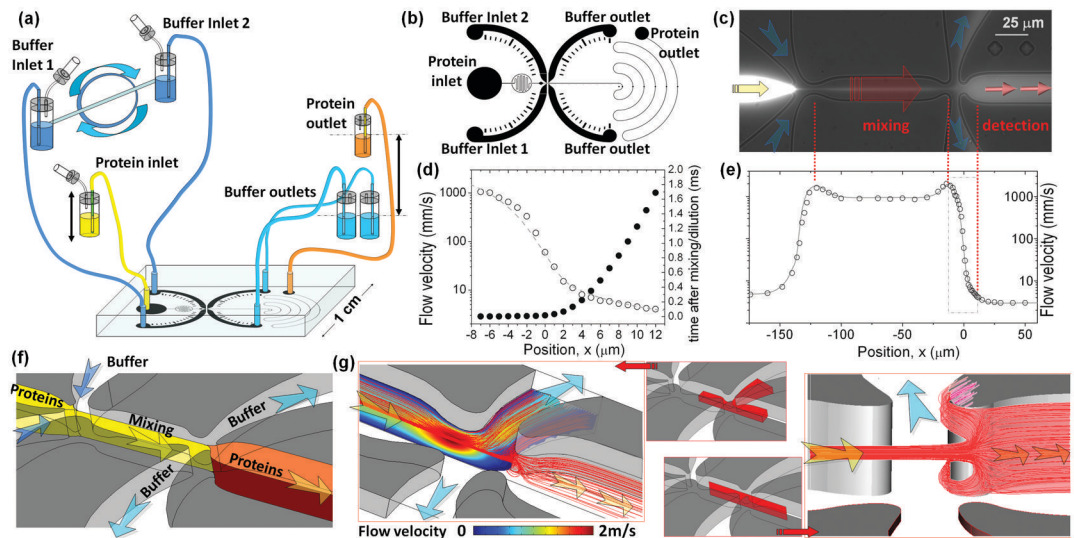
Figure 1. Microfluidic setup for kinetic smFRET measurements

(**a**) After passing through a mixing region, the protein stream and two buffer streams (fed from three separate inlets) are directed to three outlets, which are connected to separate reservoirs, whose heights are adjusted to tune mixing and dilution (see Supplementary Note). (**b**) Diagram of the device showing inlets and outlets. (**c**) Micrograph of the functional region with a fluorescent solution fed to the protein inlet. Arrows indicate buffer flow (blue), protein flow before mixing (yellow), and protein flow in mixing and detection regions (red). (**d**) Flow velocity (hollow circles), as measured with fluorescence correlation spectroscopy (FCS), and time after mixing or dilution (solid circles), both as functions of the position along the channel in the deceleration region; dashed line is from 3D flow simulations (COMSOL). (**e**) Flow velocity (as in (d)) in the focusing, mixing and deceleration regions. (**f**) Flow diagram: the protein stream is squeezed horizontally by two buffer streams for medium exchange and then directed to smFRET detection region. (**g**) Simulations of flow velocities and streamlines in two device regions highlighted in insets.
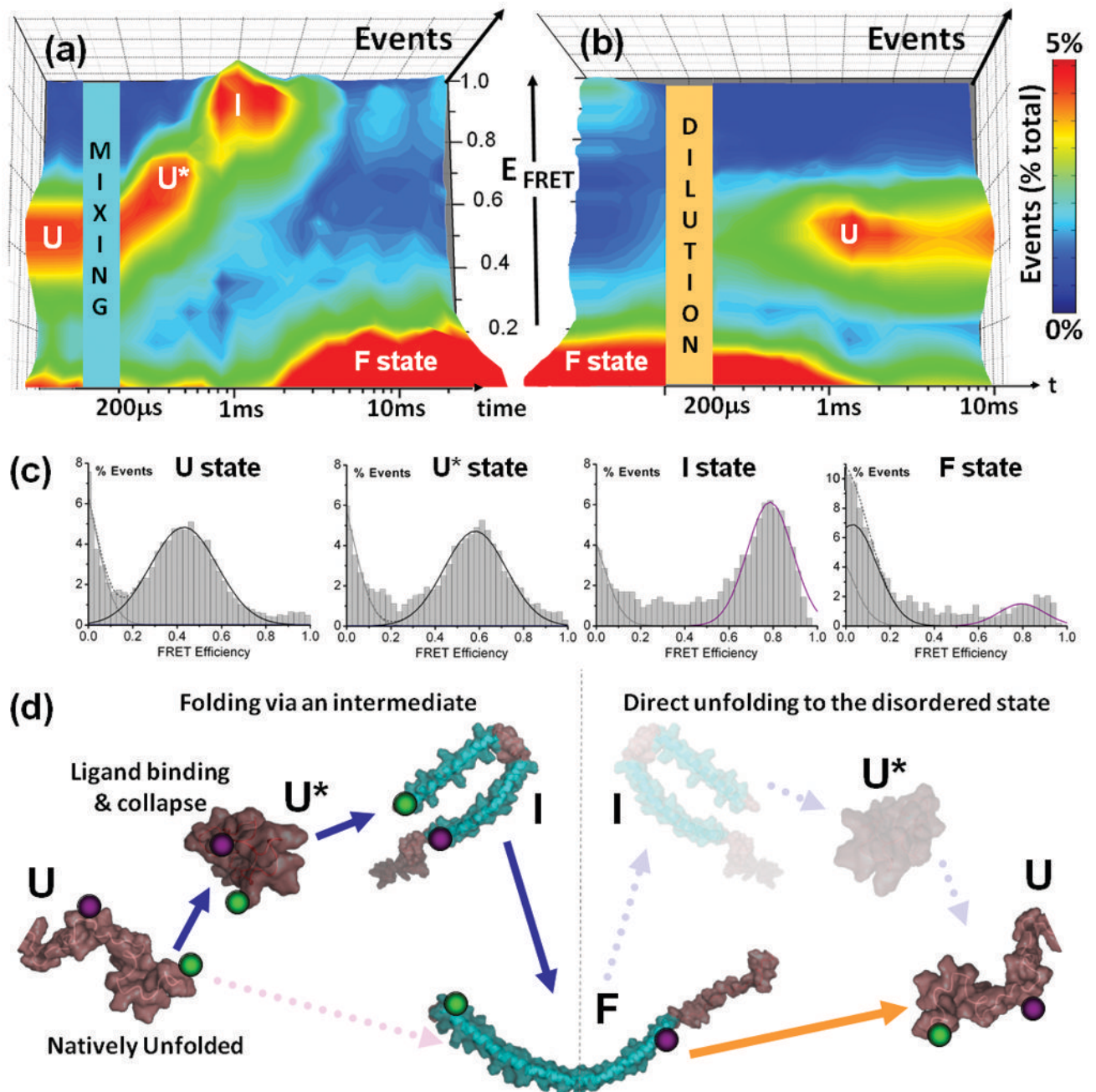
Figure 2. Folding and unfolding of α-synuclein

(**a**)α-synuclein in its intrinsically disordered **U**-state is mixed with a buffer containing SDS, triggering folding of α-synuclein into **F**-state, and smFRET is measured as the folding progresses in time. Histograms (~50,000 events) of smFRET efficiency, E_{FRET}, obtained at different time points are used to generate a 3D histogram in coordinates of time and E_{FRET}, with the percentage of total events color-coded from blue (0) to red (>5%). (**b**)Similarly plotted3D histogram for the α-synuclein unfolding reaction. The α-synuclein molecules are initially in the low-E_{FRET} **F**-state with SDS bound to the protein; massive dilution of the protein-SDS complexes triggers their dissociation and the unfolding of α-synuclein. (**c**)

Representative E_{FRET} histograms for various states: intrinsically disordered (**U**-state, E_{FRET} ≈0.42, obtained before mixing), collapsed unfolded (**U***-state, E_{FRET}≈0.6, 490 μs after mixing), intermediate (**I**-state, E_{FRET} ≈0.8, 1.2 ms after mixing), and extended structures (**F**-state, E_{FRET} ≈0.1, >10ms after mixing). (**d**) Model of the α-synuclein conformational transitions; the mirror representation emphasizes the asymmetry between the folding and unfolding pathways; the structures are color-coded (brown: disordered protein, turquoise: α-helix); green (donor) and purple (acceptor) spheres represent dye molecules.